The Journal of Immunology

RESEARCH ARTICLE | JULY 01 2014

Astrocytic TGF-β Signaling Limits Inflammation and Reduces Neuronal Damage during Central Nervous System *Toxoplasma* Infection FREE

Egle Cekanaviciute; ... et. al

J Immunol (2014) 193 (1): 139–149.
https://doi.org/10.4049/jimmunol.1303284

Astrocytic TGF-β Signaling Limits Inflammation and Reduces Neuronal Damage during Central Nervous System *Toxoplasma* Infection

Egle Cekanaviciute,*,† Hans K. Dietrich,‡,§ Robert C. Axtell,* Aaron M. Williams,* Riann Egusquiza,* Karen M. Wai,* Anita A. Koshy,*,‡,§,¶,‖,1 and Marion S. Buckwalter*,#,1

The balance between controlling infection and limiting inflammation is particularly precarious in the brain because of its unique vulnerability to the toxic effects of inflammation. Astrocytes have been implicated as key regulators of neuroinflammation in CNS infections, including infection with *Toxoplasma gondii*, a protozoan parasite that naturally establishes a chronic CNS infection in mice and humans. In CNS toxoplasmosis, astrocytes are critical to controlling parasite growth. They secrete proinflammatory cytokines and physically encircle parasites. However, the molecular mechanisms used by astrocytes to limit neuroinflammation during toxoplasmic encephalitis have not yet been identified. TGF-β signaling in astrocytes is of particular interest because TGF-β is universally upregulated during CNS infection and serves master regulatory and primarily anti-inflammatory functions. We report in this study that TGF-β signaling is activated in astrocytes during toxoplasmic encephalitis and that inhibition of astrocytic TGF-β signaling increases immune cell infiltration, uncouples proinflammatory cytokine and chemokine production from CNS parasite burden, and increases neuronal injury. Remarkably, we show that the effects of inhibiting astrocytic TGF-β signaling are independent of parasite burden and the ability of GFAP$^+$ astrocytes to physically encircle parasites. ***The Journal of Immunology*****, 2014, 193: 139–149.**

Astrocytes have recently gained prominence as essential mediators of the brain's innate immune response to a variety of brain insults, including infection. During brain infections, astrocytes secrete proinflammatory cytokines and express key immune receptors, such as TLRs and cytokine receptors, enabling them to mount a proinflammatory response to a number of signals (1–3). In addition, astrocytes upregulate the intermediate filament GFAP and form a physical barrier around the microbes and the infiltrating immune cells. This barrier function is a key characteristic of astrocytes during infection and serves to protect the brain from immune cell infiltration and neuronal injury (4, 5). Protecting the brain from neuroinflammation is critical, as the brain is uniquely vulnerable to the toxic effects of inflammation due to its limited regenerative capacity and its confined space (6, 7).

Given the importance of protecting the brain from inflammatory responses and the recognition that astrocytes play a critical role in this process, it is surprising how little is known in vivo about what role astrocytes might play in dampening neuroinflammation through their response to anti-inflammatory cytokines. TGF-β signaling in astrocytes is of particular interest because TGF-βs are master regulatory and primarily anti-inflammatory cytokines that are universally increased during CNS infection and injury (8–10). Whereas TGF-β is directly neuroprotective (11), it can also signal to all major brain cell types, including astrocytes (9, 11–13). In addition, astrocytic TGF-β signaling after stroke decreases neuroinflammation and preserves neuronal function (14). Thus, we hypothesized that astrocytic TGF-β signaling might be a key pathway for limiting brain inflammation during CNS infection. To test this hypothesis, we used the naturally neurotropic parasite *Toxoplasma gondii* to infect transgenic mice in which astrocytic TGF-β signaling was selectively inhibited, and then compared the inflammatory outcomes with infected wild-type (WT) littermates.

Toxoplasma is an obligate intracellular parasite that naturally establishes a chronic CNS infection in mice and humans and is known to increase CNS TGF-β expression (15). Astrocytes are known to play a critical proinflammatory role in controlling murine CNS toxoplasmosis. In vitro, astrocytes infected with *Toxoplasma* limit the intracellular growth of the parasite after stimulation with proinflammatory cytokines such as IFN-γ (16). In vivo, they express proinflammatory cytokines and chemokines that most likely both limit *Toxoplasma* growth and also attract immune cells (16–18). Astrocytes also clearly form a physical barrier by upregulating GFAP early in toxoplasmic encephalitis

*Department of Neurology and Neurological Sciences, Stanford University, Stanford, CA 94305; †Neurosciences Graduate Program, Stanford Neurosciences Institute, Stanford University, Stanford, CA 94305; ‡Division of Infectious Diseases, Department of Medicine, Stanford University, Stanford, CA 94305; §BIO5 Institute, University of Arizona, Tucson, AZ 85721; ¶Department of Neurology, University of Arizona, Tucson, AZ 85721; ‖Department of Immunobiology, University of Arizona, Tucson, AZ 85721; and #Department of Neurosurgery, Stanford University, Stanford, CA 94305

[1]A.A.K. and M.S.B. contributed equally to this work.

Received for publication December 10, 2013. Accepted for publication April 21, 2014.

This work was supported by a National Institutes of Health–National Institute of Diabetes and Digestive and Kidney Diseases Stanford Digestive Disease Center pilot/feasibility grant (to M.S.B.), National Institute of Neurological Disorders and Stroke Grant R01 NS067132 (to M.S.B.), a Stanford Institute for Immunity, Transplantation and Infection faculty seed grant (to M.S.B.), National Institute of Neurological Disorders and Stroke Grant K08 NS065116 (to A.A.K.), and a Stanford graduate fellowship (to E.C.).

Address correspondence and reprint requests to Dr. Marion S. Buckwalter or Dr. Anita A. Koshy, Departments of Neurology and Neurological Sciences and Neurosurgery, Stanford University School of Medicine, 1201 Welch Road, Stanford, CA 94305-5489 (M.S.B.) or Departments of Neurology and Immunobiology and the BIO5 Institute, University of Arizona, 1657 East Helen Street, Tucson, AZ 85721-0240 (A.A.K.). E-mail addresses: marion.buckwalter@stanford.edu (M.S.B.) or akoshy@email.arizona.edu (A.A.K.)

The online version of this article contains supplemental material.

Abbreviations used in this article: eGFP, enhanced GFP; qPCR, quantitative PCR; tTA, tetracycline transactivator; wpi, wk postinfection; WT, wild-type.

and physically surrounding *Toxoplasma* and leukocyte infiltrates (17, 19).

Numerous studies have shown that GFAP$^+$ astrocytes surround sites of CNS infection and inflammation and that, when there are fewer GFAP$^+$ astrocytes, infection and inflammation become more diffuse (5, 17, 19, 20). GFAP knockout mice infected with *Toxoplasma* exhibit an exacerbated brain parasite burden, an increased immune response, and an increased mortality (19). *Toxoplasma* infection produces a similar phenotype in transgenic mice that lack astrocytic gp130, a cytokine receptor that mediates the signaling of the IL-6 cytokine family (17). However, potential anti-inflammatory functions of astrocytes during *Toxoplasma* infection are poorly understood.

We report in this study that TGF-β signaling is activated in astrocytes during toxoplasmic encephalitis and that inhibition of astrocytic TGF-β signaling increases immune cell infiltration, uncouples proinflammatory cytokine and chemokine production from CNS parasite burden, and increases neuronal injury. Remarkably, we show that the effects of inhibiting astrocytic TGF-β signaling are independent of parasite burden and the ability of GFAP$^+$ astrocytes to physically encircle parasites and support the notion that astrocytes play a critical role in targeting the adaptive immune response to sites of infection.

Materials and Methods

Mice

Animal experiments were performed in compliance with the National Institutes of Health *Guide for Care and Use of Animals* and were approved by the Stanford University and University of Arizona Institutional Animal Care and Use Committees and the National Institutes of Health *Guide for Care and Use of Animals*. Ast-Tbr2DN transgenic mice were double-transgenic mice bred from B6.FVB-Tg(tetO-EGFP,-Tgfbr2)8Mcle/J (JAX 005738) and B6.Cg-Tg(GFAP-tTA)110Pop/J (JAX 005964). All experiments were done using 3-mo-old males. Singly-transgenic B6.FVB-Tg (tetO-EGFP,-Tgfbr2)8Mcle/J littermates were used as WT controls.

T. gondii *infection*

Type II (Prugniaud) parasites expressing mCherry were maintained and purified, as previously described (21). Experimental mice were orally infected with *Toxoplasma* cysts, as previously described (22). In brief, Ast-Tbr2DN or WT mice were starved overnight and then placed in individual cages and offered mouse chow soaked in brain homogenates that contained 150–180 *Toxoplasma* cysts. The mice remained in the individual cage until all of the homogenate was eaten (<3 h). In each experiment, the same number of cysts was fed to WT and Ast-Tbr2DN mice. The brain homogenates containing cysts were derived from female CBA/J mice that had been infected with 2.5×10^4 parasites i.p. 3 wk prior to harvest. Orally infected mice were sacrificed at 2 or 4 wk postinfection (wpi).

Perfusion and brain processing for immunohistochemistry

Mice were anesthetized with a ketamine/xylazine mixture (24 and 4.8 mg/ml, respectively) and terminally perfused with 0.9% NaCl containing 10 U/ml heparin. Brains were fixed in 4% paraformaldehyde in phosphate buffer for 24 h, rinsed with PBS, then sunk in 30% sucrose in PBS. Using a freezing sliding microtome (Microm HM430), 40-μm–thick, free-floating sagittal brain sections were cut into 24 sequential tubes, so that each tube contained every 24th section spaced 960 μm apart. Sections were stored in cryoprotective medium at −20°C.

Immunohistochemistry

Immunohistochemistry was performed using standard techniques (9), including no-primary Ab controls for each Ab. We used the following primary Abs for immunohistochemistry: anti-phosphorylated Smad2 (rabbit, 1:200; Millipore, AB3849), anti-enhanced GFP (eGFP; chicken, 1:200; Millipore, AB16901), anti-GFAP (rat, 1:10,000; Invitrogen, 12-0300), anti-GFAP (rabbit, 1:1,000; Dako, Z0334), biotinylated anti-GFAP (1:200, Abcam; ab79203), biotinylated anti-NeuN (mouse, 1:200; Millipore, MAB377B), anti-MAP2 (mouse, 1:200; Sigma-Aldrich, M2320; biotinylated using Thermo Scientific Pierce EZ-Link Micro Biotinylation kit, PI-21935), anti-CD68 (rat, 1:1,000; Serotec, MCA1957S), anti-CD3 (hamster, 1:500; BD Biosciences, 550277), anti-CCL5 (goat, 1:200; R&D Systems, AF478), and anti–NF-κB p65 (rabbit, 1:200; Santa Cruz Biotechnology, sc-372).

We used the following secondary Abs for immunohistochemistry: Alexa Fluor-405 goat anti-rabbit (Invitrogen, A-31556), Alexa Fluor-488 donkey anti-chicken (Jackson ImmunoResearch Laboratories, 703-096-155), Alexa Fluor-555 streptavidin (Invitrogen/Molecular Probes, S-32355), Alexa Fluor-555 donkey anti-rabbit (Invitrogen, A31572), Alexa Fluor-647 donkey anti-rabbit (Invitrogen, A-31573), Alexa Fluor-647 streptavidin (Invitrogen/Molecular Probes, S-21374), Alexa Fluor-647 donkey anti-rat (Jackson ImmunoResearch Laboratories, 712-606-153), biotinylated rabbit anti-rat (Vector Laboratories, BA-4001), biotinylated rabbit anti-goat (Vector Laboratories, BA-5000), and biotinylated goat anti-hamster (Vector Laboratories, BA-9100). All fluorescent Abs were used at 1:200, and all biotinylated secondary Abs at 1:500. 3,3′-Diaminobenzidine was used to detect biotinylated Abs. Primary anti-CCL5 Ab was used with secondary biotinylated rabbit anti-goat Ab and streptavidin-555 in sequence.

Image analysis

Images were obtained using 10× lens and 40× oil lens on a Leica TCS SPE confocal microscope, or 10× lens on an upright fluorescence microscope (Zeiss Axio Imager M1 with charge-coupled device camera). Images were analyzed using MetaMorph or ImageJ software. All colocalization studies were performed in three images per section in two sagittal sections per mouse, spaced 480 μm apart. Image acquisition, processing, and analysis were uniformly done blinded to genotype. For colocalization of p-Smad2, CCL5, or NF-κB p65 with GFAP and eGFP, markers were scored according to their colocalization with GFAP prior to assessing eGFP expression. CD68, CD3, NeuN, and MAP2 immunostaining was quantified in five sagittal sections per mouse 480 μm apart, tracing the entire cortex for NeuN and MAP2, and using representative image per section for CD68. GFAP expression was quantified in two sagittal sections per mouse 960 μm apart. Six to 10 animals per genotype were used for all image analysis and quantification experiments.

Stereology

Brain sections were stained for CD3$^+$ cells using Abs listed above and detected with diaminobenzidine. The number of CD3$^+$ cells was quantified by analyzing digital images collected using SimplePCI software (Hamamatsu, Sewickley, PA) on an Olympus IMT-2 inverted light microscope. For each section, 12 fields of view were randomly sampled throughout the cortex, beginning with the frontal cortex and moving posteriorly. We used a computerized threshold to detect only the CD3$^+$ Ab staining. All quantifications were made in five sagittal sections per mouse 480 μm apart, using 6–10 animals per genotype.

Flow cytometry

We performed flow cytometry on whole-hemisphere tissue samples using six animals per genotype. We mechanically dissociated and digested tissue using 1 ml/hemisphere collagenase D (Roche, 11-088-874-103) with 5 μl/hemisphere DNase I (Sigma-Aldrich, AMP-D1) for 1 h at 37°C. Cells were passed through a 70-μm cell strainer, isolated on a 70/40% Percoll gradient (Sigma-Aldrich, P1644), and blocked using Fc block (BioLegend, 101302). Cells were then stimulated with PMA (Sigma-Aldrich, P8139), ionomycin (Sigma-Aldrich, I3909), and GolgiStop (BD Biosciences, 554724) for 4 h and surface stained with fluorochrome-labeled Abs against CD3, CD4, and CD8 (BD Biosciences). For intracellular IFN-γ and IL-17 staining, cells were surface stained with anti-CD3; then fixed and permeabilized with Cytofix/Cytoperm (BD Biosciences, 554714); and stained with fluorochrome-labeled Abs against IFN-γ and IL-17 (BD Biosciences). The data were collected using FACScan (BD Biosciences) and analyzed using FlowJo software (Tree Star). T cell subsets were analyzed by gating on lymphocytes defined by forward scatter and side scatter profile, followed by gating on CD3. The CD3$^+$ population was then gated on CD4, CD8, and IFN-γ expression and the CD4$^+$ population was gated on IL-17 expression. We repeated and confirmed all flow cytometry analysis for infected tissue using a similar protocol for tissue preparation and cell staining (23), except that the protocol does not use collagenase/DNase digestion or stimulation.

We also performed flow cytometry on whole-spleen tissue samples using the same preparation, but without collagenase/DNase digestion, stimulation, or intracellular staining. We surface stained the samples using fluorochrome-labeled Abs against CD3, CD4, CD8, CD25, and CD19 (BD Biosciences), as well as CD11b, CD11c, Gr1, and F4/80 (eBioscience). Immune cell subsets were gated on lymphocytes and myeloid cells defined by forward scatter and side scatter profile, followed by gating on Live/Dead

AquaAmine stain (Molecular Probes, L34957). Then lymphocytes were gated on CD3 and CD19 expression. $CD3^+$ population was further gated on CD4 and CD8 expression, and $CD4^+$ population was further gated on CD25 expression. Myeloid cells were gated on CD11b expression, followed by gating on CD11c, Gr1, and F4/80 expression. All data were collected using LSRII cytometer (BD Biosciences) and analyzed using FlowJo software (Tree Star).

Protein quantification

After perfusion, brain tissue was flash frozen and kept at −80°C. Tissue was homogenized in cell lysis buffer with Complete Mini protease inhibitor (Roche, 11836153001) and 0.1% Na_3VO_4. Samples were sonicated for 10 s and centrifuged at 14,000 rpm for 10 min, and protein concentration in the supernatant was equalized using a bicinchoninic acid protein assay kit (ThermoScientific, 23227). Multiplex luminex assay was performed by the Human Immune Monitoring Center at Stanford University (himc.stanford.edu). Each sample was measured in duplicate. Plates were read using a Luminex 200 instrument with a lower bound of 100 beads per sample per cytokine. Results were analyzed using Cluster 3.0 and visualized using JavaTreeView software. CCL5 levels were measured using a mouse CCL5 Quantikine ELISA kit (R&D Systems, MMR00) on six animals per genotype.

Quantitative real-time PCR

We isolated mRNA and performed quantitative PCR (qPCR), as previously described (24). RNA was isolated from flash frozen tissue, which was kept at −80°C until homogenization in TRIzol reagent (Invitrogen, 15596-026). Samples were ground using a vibrating pestle until dissolved, mixed with chloroform at 5:1 ratio, and centrifuged at 14,000 rpm for 15 min. Supernatant was mixed 1:1 with isopropanol and centrifuged at 14,000 rpm for 10 min. Pellets were washed with 80% ethanol three times and air dried. RNA concentration and purity were measured based on light absorbance at 260 and 280 nm using a spectrophotometer. We used RNA with a 260:280 nm ratio of at least 1.8 and concentration of at least 200 ng/μl. Any genomic DNA was digested using a DNase kit (Invitrogen, 18068-015), and mRNA was converted into cDNA using Omniscript Reverse Transcriptase kit (Qiagen, 205113) with random primers (Promega, C118A) and RNase inhibitor (Roche, N808-119), according to manufacturer's instructions.

For quantification of parasite burden, whole-brain genomic DNA was isolated using a DNeasy blood and tissue kit (Qiagen, 69504) and following the manufacturer's protocol. Genomic DNA or cDNA samples were mixed with SYBR Green reagent (Qiagen, 204143) and primers, according to manufacturer's instructions, and run on Peltier Thermal Cycler PTC-200 using Opticon Monitor 3 software. Six to 11 animals per group were used for all qPCR assays. We quantified the expression of B1 gene (forward primer, 5′-TCCCCTCTGCTGGCGAAAAGT-3′; reverse primer, 5′-AGCGTTCGTGGTCAACTATCGATTG-3′) (25), with GAPDH control (forward primer, 5′-AGGTCGGTGTGAACGGATTTG-3′; reverse primer, 5′-TGTAGACCATGTAGTTGAGGTCA-3′). Parasite DNA levels were normalized using GAPDH (to control for the amount of brain tissue). Results were calculated as previously described (26).

Cyst counts

Brain sections (2 and 4 wpi) were stained with fluorescein-labeled *Dolichos biflorus* agglutinin (Vector Laboratories, 1031), which binds sugars of the cyst wall. The number of cysts was quantified by confocal microscopy (Leica TCS SPE confocal microscope). Five sagittal sections were counted per mouse for 2 wpi samples, and four sagittal sections were counted per mouse for 4 wpi samples. These counts represented approximately one-twelfth of the brain. There were seven to nine mice per genotype for 2 wpi samples, and 11–12 mice per genotype for 4 wpi samples. For images shown in Fig. 3A and 3B, brain sections were stained with biotinylated *D. biflorus* agglutinin (1:500; Vector Laboratories, B-1035), which was then detected by use of streptavidin-Cy5 (1:200; Invitrogen, 434316).

Statistical analysis

All experimental data were acquired in a blinded and unbiased fashion. Statistical analyses were performed using Prism 6 software. Means between two groups were compared using two-tailed, unpaired Student *t* test for parametric data and Mann–Whitney *U* test for nonparametric data. Means between three or more groups were compared using one-way ANOVA with Bonferroni correction for multiple comparisons for parametric data and Kruskal–Wallis test with Dunn's correction for multiple comparisons for nonparametric data. Linear correlation between *Toxoplasma* cDNA and cytokine expression was computed using Prism 6 software and expressed as R^2 and *p* value compared with zero-slope line. Weight loss between genotypes was compared using one-way repeated-measures ANOVA. Mortality was compared using Mantel–Cox log-rank test.

Results

Activated astrocytes exhibit TGF-β signaling during Toxoplasma *infection*

To verify that WT astrocytes surround *Toxoplasma* infiltrates and respond to TGF-β during acute CNS *Toxoplasma* infection, we orally infected control mice with *Toxoplasma* cysts derived from parasites that express the fluorescent protein mCherry. As expected, we observed $GFAP^+$ reactive astrocytes surrounding active sites of infection at 2 wpi (Fig. 1A). We next immunostained for p-Smad2, a readout of TGF-β signaling (27). Unsurprisingly, many cells demonstrated p-Smad2 immunostaining, and that population included $GFAP^+$ astrocytes localized around $mCherry^+$ *Toxoplasma* infiltrates (Fig. 1B). Thus, we verified that $GFAP^+$ astrocytes do exhibit TGF-β pathway activation during *Toxoplasma* infection.

Astrocytic TGF-β signaling is inhibited in the Ast-Tbr2DN mouse model

Having verified that astrocytic TGF-β signaling occurs during CNS *Toxoplasma* infection, we sought to study its functions by infecting transgenic mice in which TGF-β signaling is inhibited specifically in $GFAP^+$ astrocytes (astrocytic Tbr2 dominant-negative or Ast-Tbr2DN mice) (Fig. 2A). To engineer Ast-Tbr2DN mice, we crossed two previously described mouse lines, both of which are on a C57BL/6J genetic background and have been extensively characterized and used in other transgenic combinations (28–36). The first line (28) carries a bi-tetO promoter that, when bound by the tetracycline transactivator (tTA) protein, drives the expression of two genes, a dominant-negative mutant type II TGF-β receptor and eGFP. The type II receptor is required for all intracellular TGF-β signaling (27), and the dominant-negative mutant receptor is truncated before the kinase domain, preventing the initiation of downstream signaling when it dimerizes

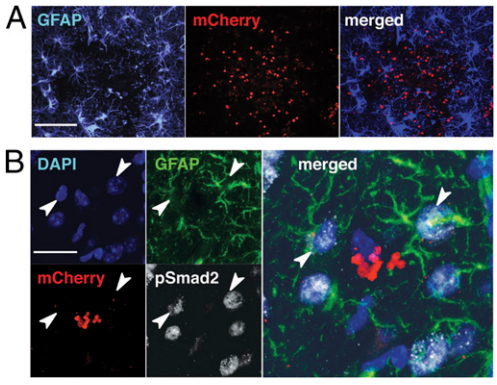

FIGURE 1. TGF-β signaling is activated in brain cells, including astrocytes during CNS toxoplasmosis. Brain sections from WT mice infected with mCherry-expressing *Toxoplasma* were stained as indicated and then examined by confocal microscopy. (**A**) Representative images showing astrocytes that immunostain for $GFAP^+$ (*left panel*, blue), $mCherry^+$ parasites (*middle panel*, red), and the merged image (*right panel*). Scale bar, 200 μm. (**B**) Representative images of p-Smad2 and GFAP coimmunostaining in areas surrounding $mCherry^+$ *Toxoplasma* infiltrates. DAPI-stained nuclei (*upper left panel*, blue), $GFAP^+$ astrocytes (*upper right panel*, green), $mCherry^+$ parasites (*lower left panel*, red), p-Smad2 staining (*lower right panel*, white), and merge of all four channels (*right panel*). Arrowheads highlight nuclei associated with the $GFAP^+$ astrocytes seen in these images. Scale bar, 20 μm.

with either another truncated receptor or a full-length native receptor. The second transgenic line expresses GFAP-tTA, which directs bi-tetO promoter-mediated expression of the truncated receptor as well as eGFP to GFAP$^+$ astrocytes (32). Single-transgenic bi-tetO mice do not express either transgene and serve as WT littermate controls.

To assess the cell specificity of transgene expression and verify downregulation of TGF-β signaling in GFAP$^+$/eGFP$^+$ astrocytes in Ast-Tbr2DN mice, we coimmunostained for p-Smad2, eGFP, and GFAP. Although we examined uninfected mice, we did not quantify transgene expression in them, because at rest cortical astrocytes do not highly express GFAP, and thus uninfected Ast-Tbr2DN mice have very few GFAP$^+$ astrocytes at baseline. Transgene expression was completely specific to astrocytes in both infected and uninfected Ast-Tbr2DN brain, and the eGFP marker was expressed in ~40% of GFAP$^+$ astrocytes 2 wk post-*Toxoplasma* infection. eGFP was not expressed in any other cell types, including monocytic or lymphocytic cells (data not shown).

Consistent with both eGFP and the mutant type II TGF-β receptor being driven by the same promoter, at 2 wpi, GFAP$^+$/eGFP$^+$ astrocytes in Ast-Tbr2DN mice were significantly less likely to immunostain for nuclear p-Smad2 than astrocytes in WT mice (40 versus 60%, respectively; Fig. 2B, 2C), indicating reduced TGF-β signaling. However, some GFAP$^+$/eGFP$^+$ astrocytes did show p-Smad2 immunostaining, which might be due to the expression of a functional, WT TGF-β receptor complex in addition to the mutant receptor. By comparison, GFAP$^+$/eGFP$^-$ astrocytes, which would be expected to express very little, if any, of the mutant receptor, were as likely to exhibit nuclear p-Smad2 as GFAP$^+$ astrocytes in WT mice, and could therefore be considered an internal control (Fig. 2C). Collectively, our data indicate that, after *Toxoplasma* infection, the mutant TGF-β receptor is coexpressed with eGFP and reduces TGF-β signaling in a significant population of Ast-Tbr2DN mouse astrocytes.

Inhibiting astrocytic TGF-β signaling has no effect on parasite burden

To study the effects of astrocytic TGF-β signaling on inflammation after *Toxoplasma* infection, we first investigated whether it might indirectly affect neuroinflammation by altering the ability of astrocytes to contain parasites or altering total parasite burden. To address these questions, we assessed the amount and distribution of *Toxoplasma* in Ast-Tbr2DN and WT mice at 2 and 4 wpi using tissue fluorescence, immunohistochemistry, and DNA-based quantification.

Gross scoring of mCherry$^+$ parasites in 2 wpi brain sections did not reveal any differences between genotypes (data not shown). In addition, at both 2 and 4 wpi (Fig. 3A, 3B), we observed that parasites formed clusters that stained for *D. biflorus* agglutinin (a marker of cysts) in the cortex of both Ast-Tbr2DN mice and WT controls and that the number of cysts did not differ between genotypes (Fig. 3C, 3D). At both time points, we further quantified parasite burden in brain homogenates by qPCR for the *Toxoplasma*-specific gene B1, a method that ensures we accounted for all parasites, even those not in cysts (25). Again, there was no difference in normalized B1 expression between genotypes at either time point (Fig. 3E, 3F). Thus, based both on direct counts and on qPCR, inhibiting astrocytic TGF-β signaling did not affect *Toxoplasma* burden or distribution in the brain during acute or chronic infection. Consistent with these findings, there was no significant difference in weight loss or mortality between the Ast-Tbr2DN and WT mice at any time point (Fig. 3G–J).

Inhibiting astrocytic TGF-β signaling increases astrocyte and myeloid cell activation during acute infection

Having verified that astrocytic TGF-β signaling does not affect parasite burden, we next evaluated whether Ast-Tbr2DN mice showed a difference in the immune response compared with WT mice. The main CNS-resident cells that participate in neuroinflammation are astrocytes and microglia, and during infection they are joined by infiltrating macrophages (17, 19, 37, 38). As GFAP upregulation is a hallmark of astrocyte activation (39), we quantified the area covered by GFAP immunostaining to measure the effects of inhibiting TGF-β signaling on astrocyte activation. In uninfected mice, we did not observe any differences in the percentage of cortical area covered by GFAP$^+$ immunostaining between Ast-Tbr2DN mice and WT controls (data not shown). However, at 2 wpi, Ast-Tbr2DN mice exhibited a ~2-fold increase in the cortical area covered by GFAP immunostaining compared with WT mice (Fig. 4A, 4B). To determine whether this increase in GFAP was related to an increase in proliferative capacity of astrocytes that lacked TGF-β signaling, we quantified the

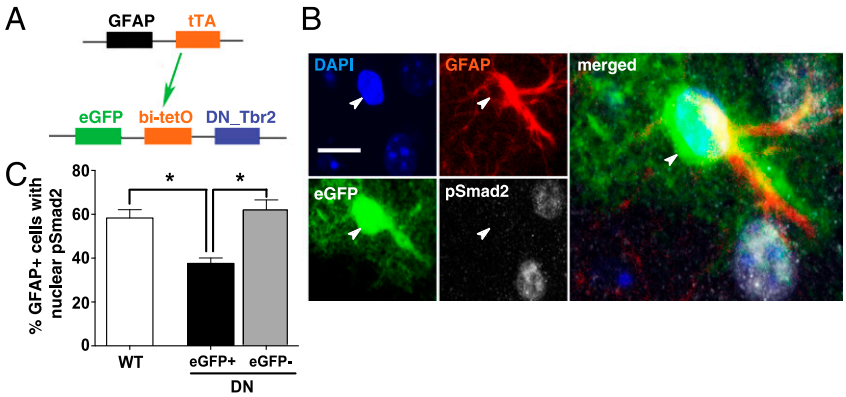

FIGURE 2. During *Toxoplasma* infection, TGF-β signaling is inhibited specifically in eGFP$^+$ astrocytes in Ast-Tbr2DN mice. (**A**) Schematic representation of the double-transgenic astrocytic Tbr2 dominant-negative mouse (Ast-Tbr2DN) line. The first transgene encodes the tTA protein, driven by a GFAP promoter. tTA binds the bidirectional bi-tetO promoter on the second transgene to stimulate expression of both eGFP and a dominant-negative mutant type II TGF-β receptor that cannot initiate downstream signaling. (**B**) Representative images of 2 wpi Ast-Tbr2DN brain section, stained as indicated. Arrowhead denotes the nucleus of the GFAP$^+$/eGFP$^+$ cell. Scale bar, 20 μm. Large image: enlargement of merged image (all four channels). (**C**) Percentage of GFAP$^+$ cells in WT or Ast-Tbr2DN brain sections that showed nuclear p-Smad2 expression at 2 wpi, as assessed by confocal microscopy. Note that, in Ast-Tbr2DN mice, the GFAP$^+$ cells are subdivided into GFAP$^+$/eGFP$^+$ and GFAP$^+$/eGFP$^-$ cells. $n = 4$ mice per genotype, 100 GFAP$^+$ cells per mouse. Bars, mean ± SEM. *$p < 0.05$, Kruskal–Wallis test with Dunn's correction for multiple comparisons.

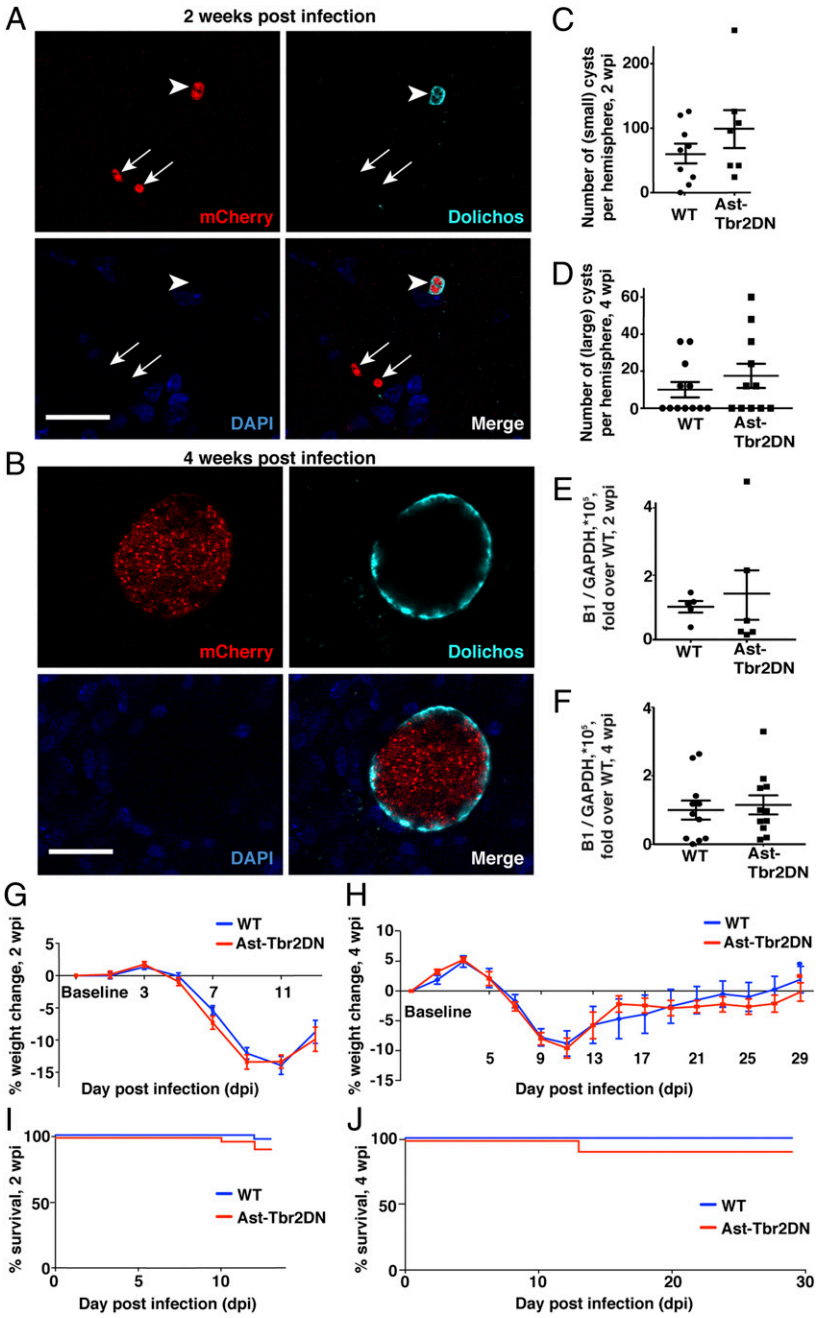

FIGURE 3. Inhibiting astrocytic TGF-β signaling does not affect *Toxoplasma* parasite burden in the brain, weight loss, or mortality. (**A**–**F**) *Toxoplasma* burden in the brain during acute (2 wpi) and chronic (4 wpi) infection. (A and B) Representative images of brain cysts at 2 wpi and 4 wpi. mCherry signal from parasites (*upper left*), *D. biflorus* agglutinin (*upper right*) that stains the cyst wall, DAPI (*lower left*), and merge (*lower right*). Arrowheads point to cysts. Arrows point to free tachyzoites (2 wpi). No free tachyzoites were seen in 4 wpi brain sections. Scale bars, 20 μm. (C and D) mCherry$^+$ Dolichos$^+$ *Toxoplasma* cysts were counted at 2 and 4 wpi. Bars, mean ± SEM. n = 7–9 mice per genotype at 2 wpi, 11–12 mice per genotype at 4 wpi. (E and F) At 2 and 4 wpi, brain homogenates were used to isolate *Toxoplasma* and mouse genomic DNA for real-time qPCR for the *Toxoplasma*-specific gene B1 and loading control GAPDH for quantification of *Toxoplasma* genomic DNA. Bars, mean ± SEM. n = 6 mice per genotype at 2 wpi, 11 mice per genotype 4 wpi. (**G** and **H**) Weight loss in Ast-Tbr2DN mice and WT controls. Bars, mean ± SEM. (G) Combined data from three independent experiments, n = 19–21 mice per genotype. (H) n = 11–12 mice per genotype. (**I** and **J**) Mortality in Ast-Tbr2DN mice and WT controls. Mantel–Cox (log-rank) test to compare mortality between genotypes. (I) Combined data from five independent experiments, n = 34 mice per genotype. (J) n = 12 mice per genotype.

colocalization of GFAP with the proliferation marker Ki67 in WT and Ast-Tbr2DN brain sections. These studies showed no genotype-specific difference in Ki67/GFAP colocalization (WT, 5.60 ± 0.79%; Ast-Tbr2DN, 8.15 ± 1.47%; p = 0.14, Student t test). In addition, there was no difference in Ki67 immunostaining in eGFP$^+$ versus eGFP$^-$ astrocytes within Ast-Tbr2DN mice (GFAP$^+$/eGFP$^+$, 8.04 ± 1.64; GFAP$^+$/eGFP$^-$, 8.17 ± 1.53; p = 0.96, Student t test) and no difference in GFAP$^+$ cell number (WT, 200.8 ± 10.8; Ast-Tbr2DN, 202.8 ± 12.8 cells per 0.34-mm^2 region; p = 0.90, Student t test). We then confirmed the GFAP increase in Ast-Tbr2DN mice by quantifying GFAP protein and mRNA expression in a separate cohort of mice 2 wpi. We observed a 1.5-fold increase in GFAP protein level in Ast-Tbr2DN compared with WT mice but no difference in mRNA levels at 2 wpi (Supplemental Fig. 1).

To investigate whether inhibiting TGF-β signaling in astrocytes affects myeloid cell activation as well, we stained for CD68, which is a marker for activated microglia and macrophages. Because CD68$^+$ cells showed significant spatial overlap in the infected cortex, we quantified their presence as the percentage of cortical area instead of attempting to count individual cells. We found that similarly to GFAP, CD68 immunostaining was not different between uninfected Ast-Tbr2DN mice and WT controls (data not shown). However, at 2 wpi, Ast-Tbr2DN mice exhibited a 2-fold increase in the cortical area covered by CD68$^+$ cells compared with WT controls (Fig. 4C, 4D). Taken together, these results demonstrate that CNS *Toxoplasma* infection induces more astrocyte and myeloid cell activation when astrocytic TGF-β signaling is inhibited.

Inhibiting astrocytic TGF-β signaling exacerbates the adaptive immune response to acute infection

As in other organs, the T lymphocyte response in the brain is the major mediator of the adaptive immune response to *Toxoplasma*

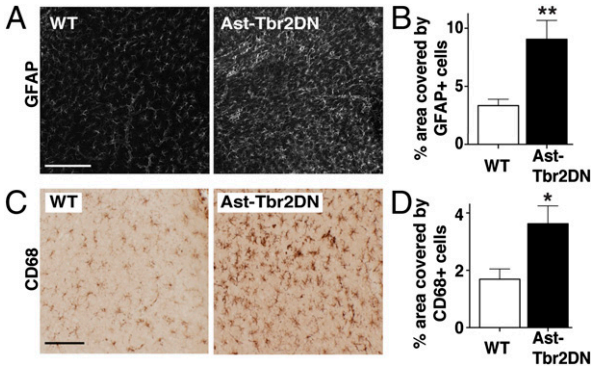

FIGURE 4. Lack of astrocytic TGF-β signaling increases the reactive astrogliosis and microglial/macrophage infiltration during acute *Toxoplasma* infection. Brain sections from 2 wpi WT or Ast-Tbr2DN mice were stained, as indicated, and examined by light microscopy. For (**B**) and (**D**), quantification was done by stereology. (**A** and B) Representative images (A) and quantification (B) of cortical area covered by GFAP$^+$ reactive astrocytes in Ast-Tbr2DN and WT mice. (**C** and D) Representative images (C) and quantification (D) of cortical area covered by CD68$^+$ activated microglia and infiltrating macrophages in Ast-Tbr2DN and WT mice. Scale bar, 200 μm. n = 7–9 mice per genotype, two images per mouse (B) and five images per mouse (D) 480 μm apart. Bars, mean ± SEM. $*p < 0.05$, $**p < 0.01$, Student t test.

infection (40). Using immunohistochemistry for the T lymphocyte marker CD3, we observed that some CD3$^+$ cells formed clusters, which have previously been shown to correspond to areas of active *Toxoplasma* infection (41), and other CD3$^+$ cells diffusely infiltrated cortical area between clusters (Fig. 5A, 5B).

Consistent with the finding of equivalent parasite burden in both groups, there was no difference in the number of CD3$^+$ clusters between genotypes (Fig. 5C). However, we observed that Ast-Tbr2DN mice showed significantly more CD3$^+$ cells diffusely infiltrating the area between the distinct clusters (Fig. 5B). To quantify this difference, we used stereology to determine an unbiased estimate of total CD3$^+$ cells in the cortex of Ast-Tbr2DN and WT mice. This verified a 2.5-fold increase in the number of CD3$^+$ cells in Ast-Tbr2DN cortex (Fig. 5D). Thus, inhibition of astrocytic TGF-β signaling not only increases the innate immune response to CNS toxoplasmosis, it also strongly increases the number of infiltrating T lymphocytes.

To investigate whether inhibiting astrocytic TGF-β signaling affects the phenotype of the adaptive immune response, we characterized T cells isolated from the brain using flow cytometry. Fig. 5E shows our gating strategy. We did not observe any differences between genotypes in the proportion of CD3$^+$ T lymphocytes that were CD4$^+$ or CD8$^+$ (Fig. 5F, 5G). Furthermore, we did not observe any differences in the percentage of CD3$^+$ T cells that expressed IFN-γ (Fig. 5H). The numbers of CD3$^+$ IL-17–expressing lymphocytes were negligible in both genotypes (data not shown).

To determine whether inhibition of astrocytic TGF-β signaling increases T cell number by promoting T cell proliferation, we quantified the percentage of proliferating CD3$^+$ T cells between genotypes by costaining sections for CD3 and Ki67 (Supplemental Fig. 2). This method again revealed an increase in T cell number, but there was no genotypic difference in the percentage of CD3$^+$ cells colocalizing with Ki67 (Supplemental Fig. 2B). Thus, inhibiting astrocytic TGF-β signaling primarily increased the number of infiltrating CD3$^+$ T cells rather than skewing their differentiation to CD4$^+$, CD8$^+$, Th1, or Th17 lymphocytes or affecting their proliferation.

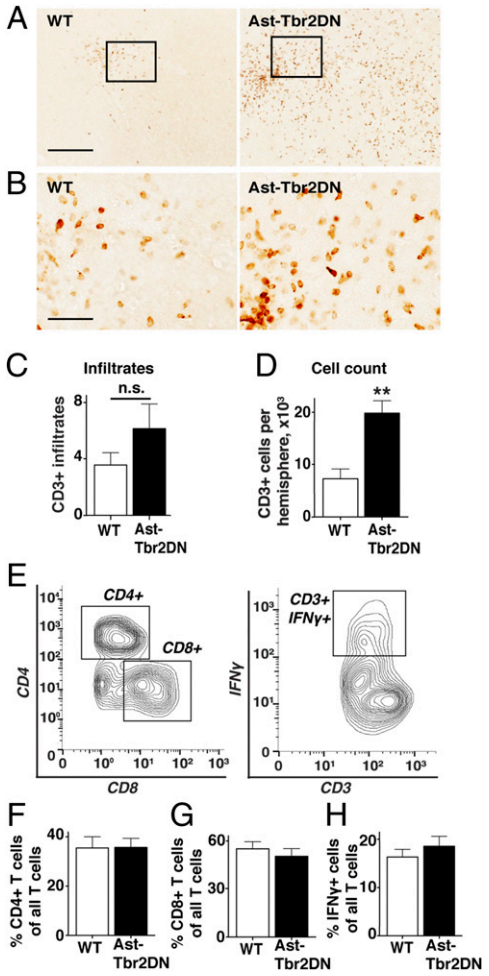

FIGURE 5. Lack of astrocytic TGF-β signaling exacerbates the T cell response to acute *Toxoplasma* infection. Brain sections from 2 wpi WT or Ast-Tbr2DN mice were stained for CD3, examined by light microscopy, and quantified using stereology. (**A**) Representative images of CD3$^+$ cells in the cortex of Ast-Tbr2DN and WT mice. Scale bar, 200 μm. (**B**) Enlargement of boxed area of (A). Scale bar, 50 μm. (**C**) Numbers of discrete CD3$^+$ cortical infiltrates in Ast-Tbr2DN and WT mice as quantified by two observers using light microscopy. n = 7–9 mice per genotype. (**D**) Stereology was used to quantify the total counts of CD3$^+$ cells in cortex of Ast-Tbr2DN and WT mice. n = 5 sections per mouse 480 μm apart, 7–9 mice per genotype. (**E**–**H**) At 2 wpi, T cell lymphocytes were isolated from Ast-Tbr2DN and WT mice and analyzed by flow cytometry for the percentage of CD4$^+$, CD8$^+$, and CD3$^+$IFN-γ$^+$ cells. (E) A representative analysis of the CD3$^+$ cells isolated from the brain homogenate of a single mouse. (F–H) Quantification of percentage of CD3$^+$ cell populations that are CD4$^+$ (F) and CD8$^+$ (G) in Ast-Tbr2DN and WT mice. (H) Quantification of percentage of CD3$^+$ cell population that is IFN-γ$^+$ in Ast-Tbr2DN mice and WT controls. n = 6 mice per genotype. Bars, mean ± SEM. $**p < 0.01$, Student t test.

To ensure that the numerical difference in the Ast-Tbr2DN CNS was not secondary to a baseline difference in Ast-Tbr2DN versus WT mice, and to determine whether the effects of inhibiting astrocytic TGF-β signaling were confined to the CNS, we used flow cytometry to measure splenic immune cells in uninfected and *Toxoplasma*-infected Ast-Tbr2DN and WT mice. In the uninfected Ast-Tbr2DN and WT mice, we found no baseline differences in the spleen immune cell populations that we characterized, as follows: dendritic cells (CD11b$^+$/CD11c$^+$/Gr1$^-$/F4/80$^-$), macrophages (CD11b$^+$/F4/80$^{+/}$CD11c$^-$/Gr1$^-$), granulocytes (CD11b$^+$/Gr1$^+$/CD11c$^-$/F4/80$^-$), CD4$^+$ T cells (CD3$^+$/CD4$^+$), CD8$^+$ T cells

($CD3^+/CD8^+$), regulatory T cells ($CD3^+/CD4^+/CD25^+$), and B cells ($CD19^+$) (Supplemental Table I). Similarly, we found no difference in splenic T cell populations between WT controls and infected Ast-Tbr2DN mice, as follows: $CD4^+$ cells (WT, 60.68 ± 1.65; Ast-Tbr2DN, 62.49 ± 0.82), $CD8^+$ cells (WT, 27.17 ± 1.36; Ast-Tbr2DN, 27.79 ± 0.72), $CD3^+/CD4^+/IFN\text{-}\gamma^+$ Th1 cells (WT, 5.13 ± 0.79; Ast-Tbr2DN, 4.85 ± 0.54), and $CD3^+/CD4^+/IL\text{-}17^+$ Th17 cells (WT, 0.10 ± 0.02; Ast-Tbr2DN, 0.13 ± 0.03).

In addition, we used a multiplex luminex platform to analyze the expression of 26 mouse cytokines and chemokines in serum from Ast-Tbr2DN and WT mice 2 wk after *Toxoplasma* infection. Again, we did not observe any differences between genotypes (Supplemental Table IIA). Thus, we found no evidence of changes in the immune response at baseline or outside the CNS in infected Ast-Tbr2DN mice. Collectively, these data show that inhibiting astrocytic TGF-β signaling influences the number but not the subtypes of T lymphocytes responding to CNS toxoplasmosis and that this difference only occurs in the CNS.

Inhibiting astrocytic TGF-β signaling increases astrocytic NF-κB activation

Prior studies have indicated that a major mechanism by which TGF-β reduces the immune response is by inhibiting the activation and nuclear translocation of the proinflammatory transcription factor NF-κB (42, 43). If the NF-κB pathway were similarly inhibited by TGF-β in astrocytes during a *Toxoplasma* infection, we would expect an increase in NF-κB signaling only in $GFAP^+$/$eGFP^+$ astrocytes in Ast-Tbr2DN mice. To test this, we quantified the percentage of $GFAP^+$ astrocytes that exhibited nuclear localization of the NF-κB subunit p65, because its nuclear translocation is a marker of NF-κB activation (44). In Ast-Tbr2DN mice, we observed a significantly higher proportion of $GFAP^+/eGFP^+$ astrocytes with nuclear NF-κB p65 immunostaining, compared with WT $GFAP^+$ astrocytes (80 versus 40%, respectively; Fig. 6).

$GFAP^+/eGFP^-$ astrocytes in Ast-Tbr2DN mice, which do not express transgene at detectable levels and show WT TGF-β signaling (Fig. 2C), showed the same probability of immunostaining for nuclear NF-κB p65 as WT astrocytes. Thus, consistent with the prior studies that have linked TGF-β signaling with inhibition of NF-κB signaling, $GFAP^+/eGFP^+$ astrocytes in Ast-Tbr2DN mice that exhibit less TGF-β signaling also exhibit more astrocytic NF-κB pathway activation.

Increased NF-κB activation is associated with astrocytic CCL5 expression in Ast-Tbr2DN mice

The NF-κB signaling pathway is associated with proinflammatory cytokine production and activation of both innate and adaptive immune responses (45). Therefore, we screened a panel of pro- and anti-inflammatory cytokines and chemokines in the cortex of Ast-Tbr2DN mice and WT controls at 2 wpi.

Surprisingly, there was no significant genotypic difference in the level of the majority of these cytokines until we took into account the intermouse variability in *Toxoplasma* burden (Fig. 3). We correlated the *Toxoplasma* burden in each mouse, as measured by *Toxoplasma* DNA content, with that mouse's brain cytokine expression. This method allowed us to take into consideration the variability of infection rates between individual mice within the same genotype. We observed that in WT mice there was a strong linear correlation between *Toxoplasma* burden and the expression of the major Th1 cytokines IFN-γ, IL-1α, IL-6, and IL-12p40, as well as the T cell chemoattractants CCL5 and CXCL10, and myeloid cell chemoattractants CCL2 and CXCL1 (blue dots, Fig. 7A–H). In marked contrast, the levels of proinflammatory cytokines and chemokines in Ast-Tbr2DN mouse brain were not

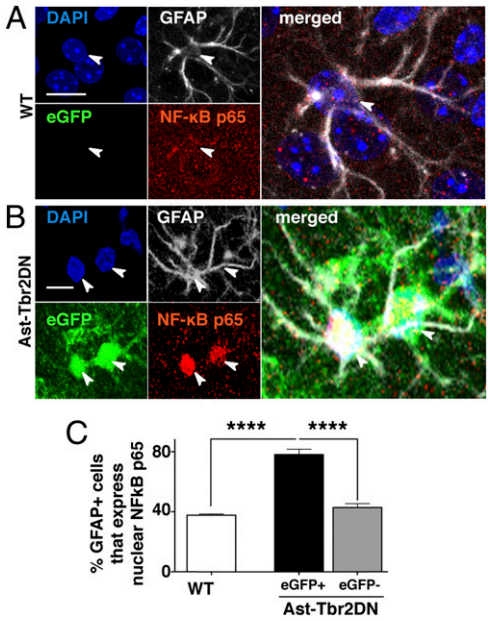

FIGURE 6. Lack of astrocytic TGF-β signaling increases NF-κB pathway activation in $eGFP^+$ astrocytes. (**A** and **B**) Representative images of 2 wpi WT (A) and Ast-Tbr2DN (B) brain sections, stained as indicated. Arrowheads denote the nuclei of the associated $GFAP^+$ cells. (**C**) Quantification of percentage of $GFAP^+$ astrocytes that immunostain for nuclear NF-κB p65 in WT and Ast-Tbr2DN mice. Note that in Ast-Tbr2DN mice the $GFAP^+$ cells are subdivided into $GFAP^+/eGFP^+$ and $GFAP^+/eGFP^-$ cells. Scale bars, 20 μm. $n = 6$ mice per genotype. Bars, mean ± SEM. $^{****}p < 0.0001$, one-way ANOVA with Bonferroni correction for multiple comparisons.

linearly correlated with the parasite burden and trended toward abnormally high expression for a given parasite burden (red squares, Fig. 7A–H).

This lack of correlation between proinflammatory cytokine levels and parasite burden in Ast-Tbr2DN mouse brain could be caused by an increase in proinflammatory cytokines produced by Ast-Tbr2DN astrocytes that exhibit more NF-κB activation, or could simply be a result of the increased number of activated immune cells found in the Ast-Tbr2DN mice cortex, or both.

The remaining cytokines and chemokines (IL-1β, IL-2, IL-3, IL-4, IL-6, IL-10, IL-12p70, IL-13, IL-17, IL-23, GM-CSF, G-CSF, CCL3, CCL7, CCL11, and vascular endothelial growth factor) were not linearly correlated with *Toxoplasma* burden in either genotype and were not affected by astrocytic TGF-β signaling. At 4 wpi, when a chronic CNS infection is well established and the majority of the parasites are encysted bradyzoites (Fig. 3D), none of the 26 chemokines and cytokines we measured linearly correlated with *Toxoplasma* burden, nor were any affected by astrocytic TGF-β signaling (Supplemental Table IIB).

Remarkably, CCL5 exhibited the most change and was 2.4-fold higher in Ast-Tbr2DN mice by multiplex luminex assay at 2 wpi. A significant increase was confirmed with a CCL5-specific ELISA (Fig. 7I). Given the abnormally high level of CCL5 in the Ast-Tbr2DN mouse brain and that CCL5 is a well-established chemoattractant for lymphocytes and macrophages, we sought to define which cells were producing excessive CCL5. As CCL5 can be secreted by a number of cells, including astrocytes (46), macrophages/microglia (18), and lymphocytes (47), we coimmunostained brain sections from Ast-Tbr2DN and WT mice for CCL5 and either the astrocyte marker GFAP or the activated microglia/macrophage marker CD68. In both genotypes, we found that, during acute infection, astrocytes were the primary cells that

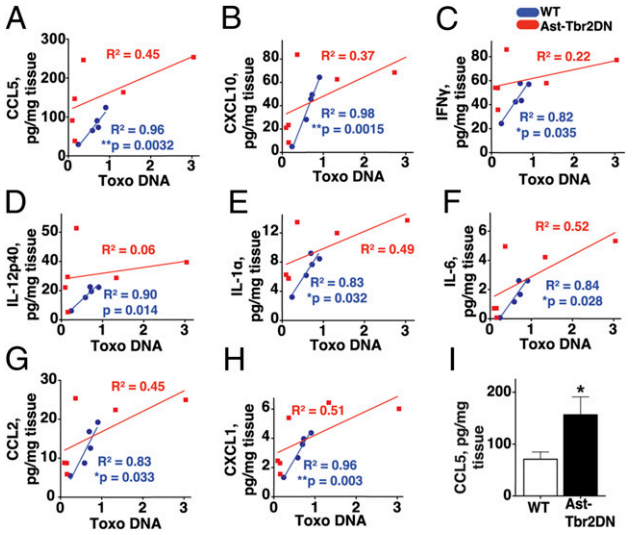

FIGURE 7. Inhibition of astrocytic TGF-β signaling leads to loss of correlation of Th1 cytokine and chemokine levels to acute CNS *Toxoplasma* burden. At 2 wpi, brain homogenates from Ast-Tbr2DN and WT mice were used to quantify multiple cytokines and chemokines via multiplex cytokine assay and *Toxoplasma* burden (measured as B1 gene DNA, normalized to GAPDH control gene DNA, and expressed as fold over WT mean) via qPCR. (**A**–**H**) Linear regressions of the *Toxoplasma* burden plotted against the levels of T cell chemokines CCL5 (A) and CXCL10 (B); Th1 cytokines IFN-γ (C), IL-12p40 (D), IL-1α (E), and IL-6 (F); and myeloid cell chemoattractants CCL2 (G) and CXCL1 (H). Blue circles, WT mice. Red squares, Ast-Tbr2DN mice. There is a statistically significant linear correlation between *Toxoplasma* load and Th1 cytokines and chemokines in WT controls (blue line), but it is lost in Ast-Tbr2DN mice (red line). (**I**) Mean CCL5 levels were approximately twice normal in Ast-Tbr2DN mouse brains. $n = 6$ mice per genotype. Bars, mean ± SEM. $^*p < 0.05$, Student t test.

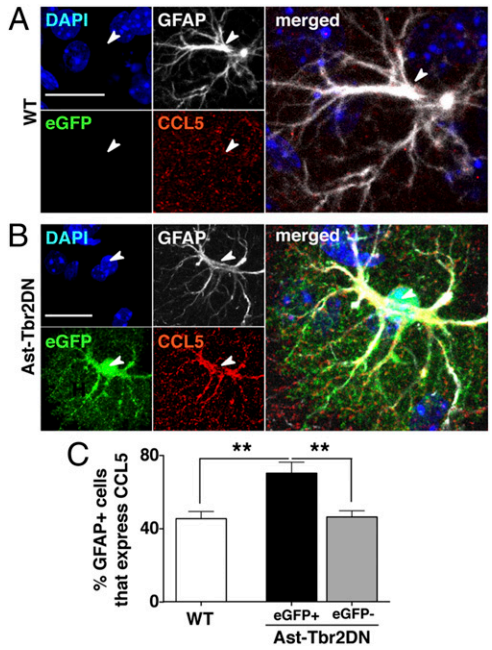

FIGURE 8. Ast-Tbr2DN mice exhibit increased immunostaining for CCL5 expression in eGFP$^+$ astrocytes. (**A** and **B**) Representative images 2 wpi from WT (A) and Ast-Tbr2DN (B) brain sections, stained as indicated. Arrowheads denote the nuclei of the associated GFAP$^+$ cells. (**C**) Quantification of percentage of GFAP$^+$ astrocytes that immunostain for CCL5 in WT controls and Ast-Tbr2DN mice. Note that in Ast-Tbr2DN mice the GFAP$^+$ cells are subdivided into GFAP$^+$/eGFP$^+$ and GFAP$^+$/eGFP$^-$ cells. Scale bars, 20 μm. $n = 6$ mice per genotype. Bars, mean ± SEM. $^{**}p < 0.01$, one-way ANOVA with Bonferroni correction for multiple comparisons.

colocalized with CCL5. Activated CD68$^+$ microglia and macrophages did not colocalize with CCL5, and we did not observe any CCL5-expressing cells that exhibited typical lymphocyte morphology (data not shown). These data suggested that, in our model, regardless of genotype, astrocytes were the primary producers of CCL5 in acute CNS infection with *Toxoplasma*.

We hypothesized that there might be a direct link between astrocytic TGF-β signaling and CCL5 expression in Ast-Tbr2DN mice in vivo, because previous in vitro studies have shown that TGF-β can inhibit astrocytic production of CCL5 (48, 49). To evaluate this possibility, we determined the percentage of GFAP$^+$ cells that coimmunostained with CCL5 in WT and Ast-Tbr2DN mice. Consistent with our hypothesis, we found that GFAP$^+$/eGFP$^+$ astrocytes were 1.5 times more likely to immunostain for intracellular CCL5 than GFAP$^+$ astrocytes in WT mice (Fig. 8). Again, GFAP$^+$/eGFP$^-$ astrocytes in Ast-Tbr2DN mice served as an internal control and were as likely to immunostain for CCL5 as WT astrocytes. This higher probability of immunostaining for CCL5 in astrocytes with inhibited TGF-β signaling is consistent with a direct link between TGF-β signaling and inhibition of CCL5 production in astrocytes in vivo.

Inhibiting astrocytic TGF-β signaling increases neuronal injury during Toxoplasma *infection*

Finally, to evaluate whether this excessive inflammation in Ast-Tbr2DN mice correlated with an increase in tissue damage, we quantified neuronal injury in Ast-Tbr2DN mice and WT controls at two time points: 2 wpi (acute stage) and 4 wpi (chronic stage). To assess neuronal injury and damage, we immunostained for two neuronal markers, as follows: MAP2, which labels dendrites, and NeuN, which labels neuronal nuclei. We then used light microscopy to evaluate the neocortex for loss of staining in WT or Ast-Tbr2DN mice. Ast-Tbr2DN mice showed significantly reduced MAP2 immunostaining at both 2 and 4 wpi consistent with an increase in dendritic injury (Fig. 9A, 9B). In addition, by 4 wpi, Ast-Tbr2DN mice exhibited significantly reduced NeuN immunostaining and disturbed cortical architecture consistent with more neuronal nuclear damage (Fig. 9C, 9D). Astrocyte loss, as assessed by GFAP staining, did not occur within these areas (Fig. 9E). Thus, the increased inflammation in Ast-Tbr2DN mouse brain was associated with both excessive dendritic loss and neuronal death in chronic toxoplasmic encephalitis. We conclude that astrocytic TGF-β signaling reduces neuroinflammation and neuronal damage during CNS *Toxoplasma* infection, and propose a model (Fig. 10) in which astrocytic TGF-β signaling inhibits the immune response by downregulating astrocytic NF-κB signaling and CCL5 production.

Discussion

In this study, we sought to determine whether astrocytic TGF-β signaling was important in directly inhibiting the neuroinflammatory response to CNS toxoplasmosis. To do this, we used *Toxoplasma* to infect a transgenic mouse model in which TGF-β signaling is inhibited specifically in a significant portion of GFAP$^+$ cells. We demonstrate in this study that inhibiting TGF-β signaling in GFAP$^+$ astrocytes did not affect *Toxoplasma*'s ability to enter or persist in the brain, but it did increase innate immune cell infiltration and activation, and adaptive immune cell infiltration early in CNS infection. Unlike WT mice in which proinflammatory cytokine and chemokine levels were tightly correlated to parasite

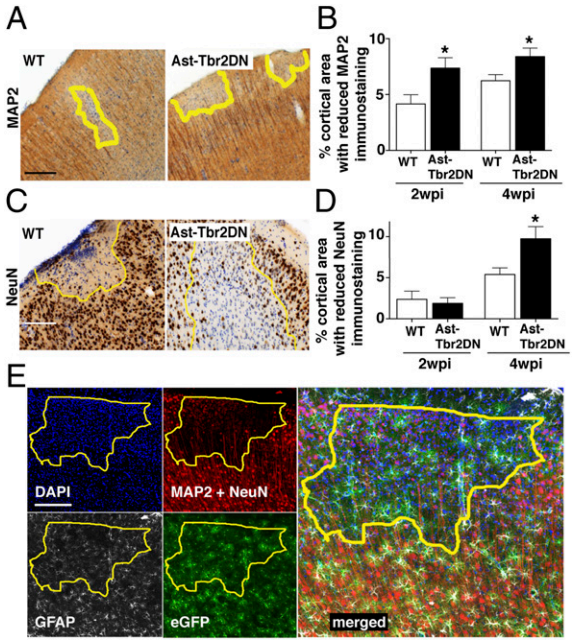

FIGURE 9. Inhibiting astrocytic TGF-β signaling increases neuronal damage during *Toxoplasma* infection. The 2 and 4 wpi Ast-Tbr2DN and WT brain sections were stained as indicated and examined by light microscopy. (**A** and **C**) Representative images of loss of MAP2 (A) or NeuN (C) staining in Ast-Tbr2DN or WT brain sections at 4 wpi. Yellow line represents area observed to have loss of stain. (**B** and **D**) Quantification of the percentage of cortical areas denoted to have loss of MAP2 (B) or NeuN (D) staining in Ast-Tbr2DN or WT mice. (**E**) Representative images of $eGFP^+/GFAP^+$ astrocytes in areas of neuronal damage in an Ast-Tbr2DN mouse 4 wpi. DAPI-stained nuclei (*upper left panel*, blue); neuronal markers, which are composed of $MAP2^+$ dendrites together with $NeuN^+$ neuronal nuclei (*upper right panel*, red); $GFAP^+$ astrocytes (*lower left panel*, white); $eGFP^+$ transgenic astrocytes (*lower right panel*, green); and merge of all four channels (*right panel*). Yellow line represents area observed to have loss of neuronal marker immunostaining. Scale bars, 200 μm. $n = 5$ images per mouse, six mice per genotype 2 wpi, 11–12 mice per genotype 4 wpi. Bars, mean ± SEM. In uninfected mice, there are no differences in gross neuroanatomical structures between Ast-Tbr2DN and WT littermates. $^*p < 0.05$, Student *t* test to compare with WT at same time point.

burden, Ast-Tbr2DN mice exhibited higher levels of proinflammatory cytokines and chemokines that were not correlated with parasite burden. Additionally, we show that a higher proportion of astrocytes with reduced TGF-β signaling demonstrated proinflammatory transcription factor NF-κB activation and proinflammatory chemokine CCL5 expression. Finally, inhibition of astrocytic TGF-β signaling exacerbated neuronal damage both early and late in the CNS infection.

One of the principal findings of this study is that astrocytic TGF-β signaling is a novel molecular mechanism whereby astrocytes limit the immune response to prevent excessive tissue damage after *Toxoplasma* infection. This astrocytic TGF-β–mediated mechanism for controlling immune cell infiltration is distinct from the astrocytic barrier to pathogen infiltration that had been previously described during *Toxoplasma* infection (17, 19). In our study, Ast-Tbr2DN mice exhibited more diffuse infiltration of T lymphocytes without demonstrating a decrease in the cortical area covered by $GFAP^+$ cells. Instead we observed the opposite—an increase in GFAP immunostaining.

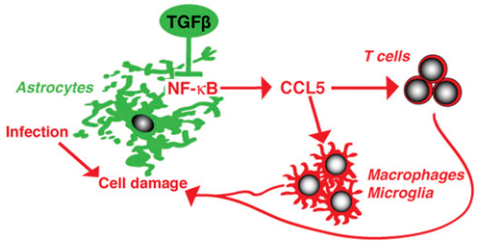

FIGURE 10. Proposed model of the functions of endogenous astrocytic TGF-β signaling during CNS *Toxoplasma* infection.

The increase in GFAP by CNS *Toxoplasma* in Ast-Tbr2DN mice was higher when measured by immunohistochemistry than by Western blot (2.5-fold versus 1.5-fold). This difference is most likely due to immunohistochemistry methods being more sensitive to changes in cellular localization, as activated astrocytes exhibit more cytoplasmic GFAP (39). It may also reflect biological variability in parasite burden (and therefore variability in GFAP upregulation) between cohorts, given that the immunohistochemistry was performed on a different cohort than qPCR and Western blots. Interestingly, we did not observe any genotype-dependent differences in GFAP mRNA levels despite a clear increase in GFAP protein in Ast-Tbr2DN mice. A likely explanation for this finding is that, because GFAP protein has a very long $t_{1/2}$ (weeks in vivo) and its $t_{1/2}$ is regulated by phosphorylation (50, 51), it is possible that astrocytic TGF-β signaling either regulates mRNA expression earlier than 2 wpi or it regulates GFAP protein stability. Finally, we did not observe any $GFAP^+$ astrocytes in either genotype that were infected with $mCherry^+$ *Toxoplasma*, indicating that astrocyte activation is unlikely to be caused by direct infection and instead is more likely to represent an increased inflammatory response to the infection.

Overall, these findings show no decrease in the physical barrier formed by astrocytes, suggesting that astrocytic TGF-β signaling does not limit neuroinflammation by strengthening the physical barrier. Instead it could be considered to induce a secretory barrier that consists of astrocytic cytokines and chemokines and ensures that immune cells target and home only to infected areas.

A major advantage of our study compared with prior in vivo studies on astrocytes and CNS toxoplasmosis is that inhibition of astrocytic TGF-β signaling did not change the acute or chronic CNS parasite load. Therefore, the differences that we found in neuroinflammation are unlikely to be driven by parasite burden and are most likely related to the change in astrocytic TGF-β signaling. By contrast, the two previous in vivo studies that examined toxoplasmic encephalitis in the setting of modified astrocytes [GFAP knockout mice and astrocytic gp130 knockout mice (17, 19)] both showed an increase in neuroinflammation and an increased CNS parasite load, making it impossible to determine whether the increase in parasite burden or the astrocytic manipulation or both drove the increase in neuroinflammation.

A second advantage of our study is that, in the transgenic Ast-Tbr2DN mice, eGFP is coexpressed with the dominant-negative type II receptor. As shown in Fig. 2, this allows us to use eGFP as a marker to determine which astrocytes have reduced TGF-β signaling and compare those astrocytes with the neighboring $eGFP^-$ astrocytes that show the same likelihood of downstream TGF-β signaling as astrocytes in the WT mice. This ability to distinguish which astrocytes have reduced TGF-β signaling at the level of a single cell enabled us to determine that it is specifically the astrocytes with reduced TGF-β signaling that are more likely to exhibit activation of the NF-κB pathway and produce CCL5. These data led us to propose that NF-κB is the molecular pathway that TGF-β utilizes in astrocytes to limit astrocytic CCL5 production. This model (Fig. 10) is consistent with previous studies that have shown that NF-κB stimulates CCL5 production in other

cell types (43, 52) and that TGF-β inhibits NF-κB activity in multiple, nonastrocyte cell types (42, 53). However, we cannot rule out the alternate possibility that the increases in NF-κB signaling and CCL5 production in astrocytes with decreased TGF-β signaling are independent of each other.

Several lines of evidence suggest that the increased CCL5 production by astrocytes is a potential mechanism that mediates increased CNS inflammation in Ast-Tbr2DN mice. CCL5 was the only cytokine of 26 cytokines assayed that was substantially different in brain homogenates from Ast-Tbr2DN mice compared with WT mice. CCL5 is a well-established chemoattractant for T lymphocytes and macrophages (47, 54), so an increase in CCL5 would be expected to attract more lymphocytes and macrophages. Finally, our observation that the $CD3^+$ T lymphocytes in the brains of Ast-Tbr2DN mice proliferate at the same rate as those in WT mice makes it unlikely that changes in T cell proliferation in the CNS account for the increased number of T lymphocytes seen in the Ast-Tbr2DN mice. These data are more consistent with the hypothesis that Ast-Tbr2DN astrocytes that lack TGF-β and have increased expression of CCL5 cause an increase in brain CCL5 levels, which in turn then recruits more T lymphocytes to the brain.

For both genotypes, our colocalization studies clearly showed CCL5 immunostaining primarily in astrocytes and not in immune cells. This finding conflicts with two previous studies from the same group that reported that immune cells produced the majority of the CCL5 in mouse brain chronically infected with *Toxoplasma* and found little CCL5 production in astrocytes (18, 55). In support of our data, astrocytic CCL5 expression has been reported during other infections in vitro (56) and in vivo (46, 57), and TGF-β has been shown to reduce CCL5 production in astrocyte cultures under proinflammatory conditions (48, 49). The discrepancies between the prior studies (18, 55) and our results may be secondary to many factors, including different techniques to examine CCL5 (protein versus mRNA), timing (2 wpi versus 30 days p.i.), different *Toxoplasma* strains, and different mouse strains.

We also report in this study that inhibiting astrocytic TGF-β signaling exacerbates neuronal damage. The Ast-Tbr2DN mice first show changes in neuronal dendritic arbors/MAP2 staining and then show loss of NeuN staining. We suspect that this increase in neuronal damage in Ast-Tbr2DN mice is directly associated with the exacerbated immune response. Indeed, inhibition of astrocytic NF-κB has been shown to be neuroprotective (58, 59). However, we cannot rule out that astrocytic TGF-β signaling also plays an independent role in neuronal protection, for example, by stimulating the production of neurotrophic molecules (60).

Finally, although we have demonstrated an important role for astrocytic TGF-β signaling, we did not investigate which cell types produced TGF-β during toxoplasmic encephalitis. Cell-specific TGF-β production could be observed by using immunohistochemistry with an anti–TGF-β Ab, but this technique would not achieve definitive results because it might also represent colocalization of TGF-β and its receptors at the cell surface or after internalization (61). However, studies in other infection and injury models have demonstrated that all CNS cell types can produce and respond to TGF-βs [reviewed in (8)]. Previous work has demonstrated that TGF-β production is indeed increased in toxoplasmic encephalitis (15) and that murine myeloid cells synthesize it when infected with *Toxoplasma* in vitro (62).

In summary, our results show that astrocytic TGF-β signaling plays an important role in how astrocytes control the neuroinflammatory response during infection. We propose a model (Fig. 10) in which endogenous astrocytic TGF-β signaling inhibits CCL5 production via the NF-κB signaling pathway and in this way reduces CCL5-mediated recruitment of macrophages and T cells to uninfected areas within the infected brain. In our model, inhibiting TGF-β signaling in a significant proportion of $GFAP^+$ astrocytes uncouples inflammation from parasite burden, perhaps because the excessive inflammation is not appropriately targeted to the invading pathogen. This excessive inflammation then leads to neuronal damage in tissue that would normally be spared. Given that TGF-β is universally upregulated during CNS inflammation, astrocytic TGF-β signaling may reflect a common pathway that induces anti-inflammatory and neuroprotective functions in astrocytes in a broad variety of CNS injuries.

Acknowledgments

We thank Dr. Yael Rosenberg-Hasson of the Stanford Human Immune Monitoring Center for technical assistance with data collection. We thank the entire Koshy, Buckwalter, and Boothroyd laboratories for helpful discussions. We thank Drs. Tonya Bliss, Brenda Porter, and Ami Okada for critical review of the manuscript.

Disclosures

The authors have no financial conflicts of interest.

References

1. Farina, C., F. Aloisi, and E. Meinl. 2007. Astrocytes are active players in cerebral innate immunity. *Trends Immunol.* 28: 138–145.
2. Ransohoff, R. M., and B. Engelhardt. 2012. The anatomical and cellular basis of immune surveillance in the central nervous system. *Nat. Rev. Immunol.* 12: 623–635.
3. Carpentier, P. A., W. S. Begolka, J. K. Olson, A. Elhofy, W. J. Karpus, and S. D. Miller. 2005. Differential activation of astrocytes by innate and adaptive immune stimuli. *Glia* 49: 360–374.
4. Wanner, I. B., M. A. Anderson, B. Song, J. Levine, A. Fernandez, Z. Gray-Thompson, Y. Ao, and M. V. Sofroniew. 2013. Glial scar borders are formed by newly proliferated, elongated astrocytes that interact to corral inflammatory and fibrotic cells via STAT3-dependent mechanisms after spinal cord injury. *J. Neurosci.* 33: 12870–12886.
5. Bush, T. G., N. Puvanachandra, C. H. Horner, A. Polito, T. Ostenfeld, C. N. Svendsen, L. Mucke, M. H. Johnson, and M. V. Sofroniew. 1999. Leukocyte infiltration, neuronal degeneration, and neurite outgrowth after ablation of scar-forming, reactive astrocytes in adult transgenic mice. *Neuron* 23: 297–308.
6. Donkin, J. J., and R. Vink. 2010. Mechanisms of cerebral edema in traumatic brain injury: therapeutic developments. *Curr. Opin. Neurol.* 23: 293–299.
7. Zipp, F., and O. Aktas. 2006. The brain as a target of inflammation: common pathways link inflammatory and neurodegenerative diseases. *Trends Neurosci.* 29: 518–527.
8. Buckwalter, M. S., and T. Wyss-Coray. 2004. Modelling neuroinflammatory phenotypes in vivo. *J. Neuroinflammation* 1: 10.
9. Doyle, K. P., E. Cekanaviciute, L. E. Mamer, and M. S. Buckwalter. 2010. TGFβ signaling in the brain increases with aging and signals to astrocytes and innate immune cells in the weeks after stroke. *J. Neuroinflammation* 7: 62.
10. Finch, C. E., N. J. Laping, T. E. Morgan, N. R. Nichols, and G. M. Pasinetti. 1993. TGF-beta 1 is an organizer of responses to neurodegeneration. *J. Cell. Biochem.* 53: 314–322.
11. Zhu, Y., G.-Y. Yang, B. Ahlemeyer, L. Pang, X.-M. Che, C. Culmsee, S. Klumpp, and J. Krieglstein. 2002. Transforming growth factor-beta 1 increases bad phosphorylation and protects neurons against damage. *J. Neurosci.* 22: 3898–3909.
12. Motizuki, M., K. Isogaya, K. Miyake, H. Ikushima, T. Kubota, K. Miyazono, M. Saitoh, and K. Miyazawa. 2013. Oligodendrocyte transcription factor 1 (Olig1) is a Smad cofactor involved in cell motility induced by transforming growth factor-β. *J. Biol. Chem.* 288: 18911–18922.
13. Arnold, T. D., G. M. Ferrero, H. Qiu, I. T. Phan, R. J. Akhurst, E. J. Huang, and L. F. Reichardt. 2012. Defective retinal vascular endothelial cell development as a consequence of impaired integrin αVβ8-mediated activation of transforming growth factor-β. *J. Neurosci.* 32: 1197–1206.
14. Cekanaviciute, E., N. Fathali, K. P. Doyle, A. M. Williams, J. Han, and M. S. Buckwalter. 2014. Astrocytic transforming growth factor-beta signaling reduces subacute neuroinflammation after stroke in mice. *Glia* DOI: 10.1002/glia.22675.
15. Hunter, C. A., J. S. Abrams, M. H. Beaman, and J. S. Remington. 1993. Cytokine mRNA in the central nervous system of SCID mice infected with *Toxoplasma gondii*: importance of T-cell-independent regulation of resistance to *T. gondii*. *Infect. Immun.* 61: 4038–4044.
16. Wilson, E. H., and C. A. Hunter. 2004. The role of astrocytes in the immunopathogenesis of toxoplasmic encephalitis. *Int. J. Parasitol.* 34: 543–548.
17. Drögemüller, K., U. Helmuth, A. Brunn, M. Sakowicz-Burkiewicz, D. H. Gutmann, W. Mueller, M. Deckert, and D. Schlüter. 2008. Astrocyte gp130 expression is critical for the control of *Toxoplasma* encephalitis. *J. Immunol.* 181: 2683–2693.

18. Strack, A., V. C. Asensio, I. L. Campbell, D. Schlüter, and M. Deckert. 2002. Chemokines are differentially expressed by astrocytes, microglia and inflammatory leukocytes in *Toxoplasma* encephalitis and critically regulated by interferon-gamma. *Acta Neuropathol.* 103: 458–468.
19. Stenzel, W., S. Soltek, D. Schlüter, and M. Deckert. 2004. The intermediate filament GFAP is important for the control of experimental murine *Staphylococcus aureus*-induced brain abscess and *Toxoplasma* encephalitis. *J. Neuropathol. Exp. Neurol.* 63: 631–640.
20. Voskuhl, R. R., R. S. Peterson, B. Song, Y. Ao, L. B. Morales, S. Tiwari-Woodruff, and M. V. Sofroniew. 2009. Reactive astrocytes form scar-like perivascular barriers to leukocytes during adaptive immune inflammation of the CNS. *J. Neurosci.* 29: 11511–11522.
21. Koshy, A. A., H. K. Dietrich, D. A. Christian, J. H. Melehani, A. J. Shastri, C. A. Hunter, and J. C. Boothroyd. 2012. *Toxoplasma* co-opts host cells it does not invade. *PLoS Pathog.* 8: e1002825.
22. Kim, S. K., A. Karasov, and J. C. Boothroyd. 2007. Bradyzoite-specific surface antigen SRS9 plays a role in maintaining *Toxoplasma gondii* persistence in the brain and in host control of parasite replication in the intestine. *Infect. Immun.* 75: 1626–1634.
23. Uhrlaub, J. L., J. D. Brien, D. G. Widman, P. W. Mason, and J. Nikolich-Zugich. 2011. Repeated in vivo stimulation of T and B cell responses in old mice generates protective immunity against lethal West Nile virus encephalitis. *J. Immunol.* 186: 3882–3891.
24. Shi, J., J. Johansson, N. S. Woodling, Q. Wang, T. J. Montine, and K. Andreasson. 2010. The prostaglandin E2 E-prostanoid 4 receptor exerts anti-inflammatory effects in brain innate immunity. *J. Immunol.* 184: 7207–7218.
25. Noor, S., A. S. Habashy, J. P. Nance, R. T. Clark, K. Nemati, M. J. Carson, and E. H. Wilson. 2010. CCR7-dependent immunity during acute *Toxoplasma gondii* infection. *Infect. Immun.* 78: 2257–2263.
26. Caffaro, C. E., A. A. Koshy, L. Liu, G. M. Zeiner, C. B. Hirschberg, and J. C. Boothroyd. 2013. A nucleotide sugar transporter involved in glycosylation of the *Toxoplasma* tissue cyst wall is required for efficient persistence of bradyzoites. *PLoS Pathog.* 9: e1003331.
27. Shi, Y., and J. Massagué. 2003. Mechanisms of TGF-beta signaling from cell membrane to the nucleus. *Cell* 113: 685–700.
28. Frugier, T., K. Koishi, K. I. Matthaei, and I. S. McLennan. 2005. Transgenic mice carrying a tetracycline-inducible, truncated transforming growth factor beta receptor (TbetaRII). *Genesis* 42: 1–5.
29. Li, F., and M. Zhou. 2013. Conditional expression of the dominant-negative TGF-β receptor type II elicits lingual epithelial hyperplasia in transgenic mice. *Dev. Dyn.* 242: 444–455.
30. Lin, H. Y., and L. T. Yang. 2013. Differential response of epithelial stem cell populations in hair follicles to TGF-β signaling. *Dev. Biol.* 373: 394–406.
31. Rani, R., A. G. Smulian, D. R. Greaves, S. P. Hogan, and D. R. Herbert. 2011. TGF-β limits IL-33 production and promotes the resolution of colitis through regulation of macrophage function. *Eur. J. Immunol.* 41: 2000–2009.
32. Pascual, O., K. B. Casper, C. Kubera, J. Zhang, R. Revilla-Sanchez, J. Y. Sul, H. Takano, S. J. Moss, K. McCarthy, and P. G. Haydon. 2005. Astrocytic purinergic signaling coordinates synaptic networks. *Science* 310: 113–116.
33. Lin, W., A. Kemper, K. D. McCarthy, P. Pytel, J. P. Wang, I. L. Campbell, M. F. Utset, and B. Popko. 2004. Interferon-gamma induced medulloblastoma in the developing cerebellum. *J. Neurosci.* 24: 10074–10083.
34. Lopez, M. E., A. D. Klein, U. J. Dimbil, and M. P. Scott. 2011. Anatomically defined neuron-based rescue of neurodegenerative Niemann-Pick type C disorder. *J. Neurosci.* 31: 4367–4378.
35. Halassa, M. M., C. Florian, T. Fellin, J. R. Munoz, S. Y. Lee, T. Abel, P. G. Haydon, and M. G. Frank. 2009. Astrocytic modulation of sleep homeostasis and cognitive consequences of sleep loss. *Neuron* 61: 213–219.
36. Florian, C., C. G. Vecsey, M. M. Halassa, P. G. Haydon, and T. Abel. 2011. Astrocyte-derived adenosine and A1 receptor activity contribute to sleep loss-induced deficits in hippocampal synaptic plasticity and memory in mice. *J. Neurosci.* 31: 6956–6962.
37. Pifer, R., and F. Yarovinsky. 2011. Innate responses to *Toxoplasma gondii* in mice and humans. *Trends Parasitol.* 27: 388–393.
38. Miller, C. M., N. R. Boulter, R. J. Ikin, and N. C. Smith. 2009. The immunobiology of the innate response to *Toxoplasma gondii*. *Int. J. Parasitol.* 39: 23–39.
39. Sofroniew, M. V., and H. V. Vinters. 2010. Astrocytes: biology and pathology. *Acta Neuropathol.* 119: 7–35.
40. Dupont, C. D., D. A. Christian, and C. A. Hunter. 2012. Immune response and immunopathology during toxoplasmosis. *Semin. Immunopathol.* 34: 793–813.
41. Ferguson, D. J., D. I. Graham, and W. M. Hutchison. 1991. Pathological changes in the brains of mice infected with *Toxoplasma gondii*: a histological, immunocytochemical and ultrastructural study. *Int. J. Exp. Pathol.* 72: 463–474.
42. Ghafoori, P., T. Yoshimura, B. Turpie, and S. Masli. 2009. Increased IkappaB alpha expression is essential for the tolerogenic property of TGF-beta-exposed APCs. *FASEB J.* 23: 2226–2234.
43. Cho, M. L., S. Y. Min, S. H. Chang, K. W. Kim, S. B. Heo, S. H. Lee, S. H. Park, C. S. Cho, and H. Y. Kim. 2006. Transforming growth factor beta 1 (TGF-beta1) down-regulates TNFalpha-induced RANTES production in rheumatoid synovial fibroblasts through NF-kappaB-mediated transcriptional repression. *Immunol. Lett.* 105: 159–166.
44. Gerondakis, S., T. S. Fulford, N. L. Messina, and R. J. Grumont. 2014. NF-κB control of T cell development. *Nat. Immunol* 15: 15–25.
45. Ben-Neriah, Y., and M. Karin. 2011. Inflammation meets cancer, with NF-κB as the matchmaker. *Nat. Immunol.* 12: 715–723.
46. Cota, M., A. Kleinschmidt, F. Ceccherini-Silberstein, F. Aloisi, M. Mengozzi, A. Mantovani, R. Brack-Werner, and G. Poli. 2000. Upregulated expression of interleukin-8, RANTES and chemokine receptors in human astrocytic cells infected with HIV-1. *J. Neurovirol.* 6: 75–83.
47. Appay, V., and S. L. Rowland-Jones. 2001. RANTES: a versatile and controversial chemokine. *Trends Immunol.* 22: 83–87.
48. Oh, J. W., L. M. Schwiebert, and E. N. Benveniste. 1999. Cytokine regulation of CC and CXC chemokine expression by human astrocytes. *J. Neurovirol.* 5: 82–94.
49. Guo, H., Y. X. Jin, M. Ishikawa, Y. M. Huang, P. H. van der Meide, H. Link, and B. G. Xiao. 1998. Regulation of beta-chemokine mRNA expression in adult rat astrocytes by lipopolysaccharide, proinflammatory and immunoregulatory cytokines. *Scand. J. Immunol.* 48: 502–508.
50. DeArmond, S. J., Y. L. Lee, H. A. Kretzschmar, and L. F. Eng. 1986. Turnover of glial filaments in mouse spinal cord. *J. Neurochem.* 47: 1749–1753.
51. Takemura, M., H. Gomi, E. Colucci-Guyon, and S. Itohara. 2002. Protective role of phosphorylation in turnover of glial fibrillary acidic protein in mice. *J. Neurosci.* 22: 6972–6979.
52. Tai, K., H. Iwasaki, S. Ikegaya, and T. Ueda. 2013. Minocycline modulates cytokine and chemokine production in lipopolysaccharide-stimulated THP-1 monocytic cells by inhibiting IκB kinase α/β phosphorylation. *Transl. Res.* 161: 99–109.
53. Haller, D., L. Holt, S. C. Kim, R. F. Schwabe, R. B. Sartor, and C. Jobin. 2003. Transforming growth factor-beta 1 inhibits non-pathogenic Gram negative bacteria-induced NF-kappa B recruitment to the interleukin-6 gene promoter in intestinal epithelial cells through modulation of histone acetylation. *J. Biol. Chem.* 278: 23851–23860.
54. Huang, W. C., F. C. Yen, F. S. Shie, C. M. Pan, Y. J. Shiao, C. N. Yang, F. L. Huang, Y. J. Sung, and H. J. Tsay. 2010. TGF-beta1 blockade of microglial chemotaxis toward Abeta aggregates involves SMAD signaling and down-regulation of CCL5. *J. Neuroinflammation* 7: 28.
55. Strack, A., D. Schlüter, V. C. Asensio, I. L. Campbell, and M. Deckert. 2002. Regulation of the kinetics of intracerebral chemokine gene expression in murine *Toxoplasma* encephalitis: impact of host genetic factors. *Glia* 40: 372–377.
56. McKimmie, C. S., and G. J. Graham. 2010. Astrocytes modulate the chemokine network in a pathogen-specific manner. *Biochem. Biophys. Res. Commun.* 394: 1006–1011.
57. Ovanesov, M. V., Y. Ayhan, C. Wolbert, K. Moldovan, C. Sauder, and M. V. Pletnikov. 2008. Astrocytes play a key role in activation of microglia by persistent Borna disease virus infection. *J. Neuroinflammation* 5: 50.
58. Brambilla, R., A. Hurtado, T. Persaud, K. Esham, D. D. Pearse, M. Oudega, and J. R. Bethea. 2009. Transgenic inhibition of astroglial NF-kappa B leads to increased axonal sparing and sprouting following spinal cord injury. *J. Neurochem.* 110: 765–778.
59. Brambilla, R., G. Dvoriantchikova, D. Barakat, D. Ivanov, J. R. Bethea, and V. I. Shestopalov. 2012. Transgenic inhibition of astroglial NF-κB protects from optic nerve damage and retinal ganglion cell loss in experimental optic neuritis. *J. Neuroinflammation* 9: 213.
60. Hahn, M., H. Lorez, and G. Fischer. 1997. Effect of calcitriol in combination with corticosterone, interleukin-1beta, and transforming growth factor-beta1 on nerve growth factor secretion in an astroglial cell line. *J. Neurochem.* 69: 102–109.
61. Di Guglielmo, G. M., C. Le Roy, A. F. Goodfellow, and J. L. Wrana. 2003. Distinct endocytic pathways regulate TGF-beta receptor signalling and turnover. *Nat. Cell Biol.* 5: 410–421.
62. Bermudez, L. E., G. Covaro, and J. Remington. 1993. Infection of murine macrophages with *Toxoplasma gondii* is associated with release of transforming growth factor beta and downregulation of expression of tumor necrosis factor receptors. *Infect. Immun.* 61: 4126–4130.